archives
of thermodynamics
Vol. **44**(2023), No. 3, 325–358
DOI: 10.24425/ather.2023.147549

Effect of artificial coarseness on the performance of rectangular solar air heater duct: a comparative study

MANOJ KUMAR DUBEY*
OM PRAKASH

National Institute of Technology Patna, Patna, Bihar 800005, India

Abstract Solar air heater is regarded as the most common and popular solar thermal system and has a wide range of applications, from residential to industrial. Solar air heater is not viable because of the low convective heat transfer coefficient at the absorber plate which contributes to decreasing the thermal efficiency. Artificial coarseness on the plain surface is the most effective method to enhance heat transfer with a moderate rate of friction factor of flowing air in the design of solar air heater duct. The different parameters and different artificial coarseness are responsible to alter the flow structure and heat transfer rate. Over the years different artificial roughness and how its geometry affects the performance of solar air heater have been thoroughly studied. Various investigators report the correlations between heat transfer and friction factors. In the present study, a comparison of several artificial coarseness geometries and methods with a view to enhancing the performance of solar air heater has been made. A brief outline has also been presented for future research.

Keywords: Solar energy; Artificial coarseness; Heat transfer coefficient; Thermo-hydraulic performance; Friction factor

Nomenclature

D	–	hydraulic diameter, mm
d	–	dimple diameter, mm
d/W	–	relative width of the gap

*Corresponding Author. Email: manojd.phd18.me@nitp.ac.in

d/D	–	relative diameter of rib print
e	–	rib height, mm
Re^+	–	roughness Reynolds number
e/D	–	relative roughness height
F'	–	flat collector efficiency factor
F_R	–	heat removal factor
f_r	–	friction factor for roughened surface
f_s	–	friction factor of flat duct
G^0	–	mass flux, kg/(s m^2)
G_d	–	distance of the gap, mm
$G(\mathrm{Re}^+)$	–	heat transfer function
$G_d/L_v,\ d/x$	–	relative position of the gap
g	–	groove position or gap, mm
g/e	–	relative gap position
g^I/e	–	relative additional gap in each symmetrical rib
g/P	–	relative groove position
H	–	duct height, mm
I	–	global solar irradiation, W/m^2
L	–	length of long way test section, mm
L_f	–	final length of duct, mm
L_v	–	length of V-rib, mm
L/e	–	relative long way length
l/s	–	relative length of metal grid rib
m^0	–	mass flow rate, kg/s
Nu	–	Nusselt number of roughened duct
Nu_s	–	Nusselt number of smooth duct
q_u	–	heat flux, W/m^2
P'	–	staggered rib position, mm
P_b/e_d	–	relative dimpled pitch
p/P	–	relative staggered rib pitch
P^I/p	–	relative staggered rib roughness
P/e	–	relative roughness pitch
ΔP	–	pressure drop, Pa
Re	–	Reynolds number
$R(\mathrm{Re}^+)$	–	momentum transfer roughness function
$r/g,\ r/e$	–	relative staggered rib size
S	–	length of short way discrete rib, mm
S/e	–	relative short way length
St	–	Stanton number
s'/s	–	dimensionless gap position
s'	–	gap position, mm
T_{fi}	–	entry temperature, K
T_{fo}	–	exit temperature, K
T_a	–	ambient temperature, K
U_L	–	overall heat loss coefficient, W/(m^{2}K)
V	–	velocity, m/s
W	–	duct width, mm
w	–	width of a single V-rib, mm
W/H	–	aspect ratio

W/w – relative roughness width
W_c/W_d – relative dimpled obstacles
w/e – staggered length of the rib to the height of the rib

Greek symbols

α – angle of inclination in flow direction, degree
Φ – chamfer angle, degree
ρ – density, kg/m^3
η – thermal efficiency
τ – transmittance

Acronyms

HVAC – heating, ventilation and air conditioning
SAH – solar air heater
THP – thermo-hydraulic performance

1 Introduction

Since the beginning of human civilization, energy has been one of the most vital factors for sustainability of the mankind. Today, energy remains an essential element of global economic growth and industrialization. With the rapidly diminishing fossil fuel reserves, which have been the primary source of energy so far, it has become imperative to find new energy sources. Solar energy has emerged as a viable source of alternative energy, which is clean, ensures a pollution-free environment, and which is available year-round. In other words, besides mitigating the energy crisis, it can also reduce CO_2 emissions. Another benefit is that solar energy is easy to change into other types of energy, such as thermal, mechanical, chemical, and electrical energy. A solar air heater (SAH) is an apparatus that absorbs solar energy and then transfers the heat energy to the air passing through. As SAH has been established as one of the most cost-effective techniques for converting solar energy, it is being widely used in various industries for room heating, room cooling, room drying, and other industrial purposes [1].

Absorber plates are an essential component of solar air heaters (SAHs). However, the formation of a viscous sublayer over the absorber plate tends to reduce the heat transfer coefficient and increase thermal resistance. The research established that artificial coarseness in the absorber plate could be an effective method to break laminar sublayers and increase the heat transfer coefficient [2]. However, it causes a significant pressure drop, enhancing the requirement for electricity. Many researchers have utilized artificial

coarseness geometry of various configurations and dimensions to enhance heat transfer and improve SAH efficiency. The present study provides an overview of different geometries, such as V-shape, W-shape, arc-shape, etc., and examines how different orientations of artificial roughness affect the performance of SAH. The aim of this paper is to determine which artificial coarseness surface works the best with different shapes and structures.

Generally, traditional SAH has low thermal performance because of a smooth surface that offers low convective heat transfer to flowing air, leading to major losses in surrounding. The SAH performance can be increased in two ways: by reducing the top surface heat loss of SAH or by enhancing the heat transfer at the absorber plate. Various methods are available to enhance the heat transfer but the most common method is to increase the heat transfer rate by using artificial coarseness instead of a smooth surface. Artificial roughness develops turbulence on a heated surface and breaks the laminar sublayer but it causes an increase in the pressure drop which is undesirable for the design of SAH. In this paper, the previous research of artificial coarseness used in SAH is summarized.

2 Theory of artificial roughness

Conventional SAHs are inefficient due to inadequate provision for heat transfer between the absorber plates and the air passage. As a result, the thermal resistance between the absorbing plates and the air is higher in the SAHs. Consequently, it increases the temperature, thereby increasing the heat loss to the surrounding area. The presence of a laminar sublayer interrupts heat exchange between the absorber plate and air passage [3]. By introducing artificial coarseness, the laminar sublayer can be broken so as to improve heat exchange by producing local turbulence. However, it can also increase the friction losses leading to an increase in the power consumption for fluid flow. Several studies revealed that Nusselt number (Nu) and friction factor (f) are also affected by factors, such as rib arrangement, wire form, rib height, and rib pitch.

3 Principle of solar air heater

In a nutshell, a traditional solar air heater absorbs solar radiation and converts it into thermal energy. As illustrated in Fig. 1, the SAH has a glass cover, a rear insulated cover, and a blower. To prevent heat transfer from

the top of the absorber plate to the surroundings, a glass cover is used, which simultaneously allows incoming solar light to pass through the absorber plate. In addition, it serves as insulation at the backside, thereby reducing the energy loss. The heated air is transported *via* a duct to the three insulated sides and a collector at the top side of the heater. SAH is utilized for various residential and industrial applications in moderate-temperature. Applications include industrial heating, ventilation and air conditioning (HVAC) systems, agricultural crop drying, and space heating. A conventional SAH loses the maximum amount of energy to the surrounding environment because energy cannot be transferred efficiently between the absorber plate and the air duct. Due to the formation of a laminar sublayer near the boundary exchanging thermal energy, its thermal performance is poor. As a result, it is essential to choose an appropriate method of heat transfer that will enhance the performance of SAH.

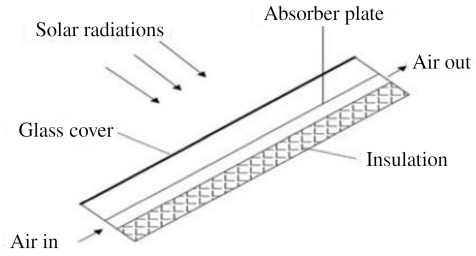

Figure 1: Schematic diagram of a solar air heater.

4 Characteristics of fluid flow and heat transfer through artificially roughened ducts in solar air heater

In the study, Nikuradse [4] used a technique called sandblasting to make the air flow more smoothly and control its temperature. He tested different levels of roughness and speed to see what works best. The 'roughness Reynolds number' (Re^{+}) is a special number that helps us understand how well a rough surface is performing in transferring heat. It is a way to figure out the best conditions for heat transfer on a rough surface.

The roughness Reynolds number is provided as

$$\mathrm{Re}^{+} = \sqrt{\frac{2}{f_r}} \left(\frac{e}{D}\right) \mathrm{Re}\,, \tag{1}$$

where f_r is the roughened surface friction factor representing the pressure loss of a fluid, e/D is the relative height, which is defined as the ratio of rib height (e) to the hydraulic diameter (D) of the duct.

As explained below, three flow regions were developed for the flow roughness:

I Hydraulic flow regime ($0 < \mathrm{Re}^+ < 5$)

For smooth pipes, the friction factor (f_s) remains constant for all values of relative height (e/D).

In the hydraulic smooth flow regime, the flow resistance in terms of friction factor is not a function of roughness height and flow behaves as laminar in such roughened pipe.

Roughness function $R(\mathrm{Re}^+)$ is defined as dimensional flow velocity at the control volume edge enclosing roughness elements. It represents momentum losses caused by roughness. The following correlation was proposed:

$$R(\mathrm{Re}^+) = \sqrt{\frac{2}{fs}} + 2.5 \ln\left(\frac{2e}{D}\right) + 3.75\,. \tag{2}$$

II Transitional flow regime ($5 < \mathrm{Re}^+ < 70$)

The effect of rib altitude can be observed in this transitional area. The roughness Reynolds number (Re^+) and the e/D ratio, which is defined as the ratio of rib height (e) to the hydraulic diameter of the duct, have an impact on the roughness behavior.

III Fully developed flow regime ($\mathrm{Re}^+ > 70$)

The roughness function (R) remains constant in the rough area. Reynolds number is unaffected by roughness. Dipprey and Sabersky [5] investigated the flow across an irregular plane of densely filled-up sand grains in a conduit by using air as the moving fluid. Heat transfer correlation for the fully developed flow region is presented as follows:

$$G(\mathrm{Re}^+) = \left(\frac{fs}{2\mathrm{St}} - 1\right)\sqrt{\frac{fs}{2}} + R\left(\mathrm{Re}^+\right). \tag{3}$$

Here, St is the Stanton number which is defined as the ratio of heat transfer of a fluid to the thermal capacity of a fluid, and D is the hydraulic diameter of the duct which is generally defined for a non-circular duct. The roughness function is defined as for fully developed flow region (Eq. (3)).

Heat transfer function $G\left(\mathrm{Re}^{+}\right)$ represents dimensionless temperature difference over the same control volume. It signifies the heat transfer capacity of a rough surface.

In addition to the analytical model, some researchers studied the heat transfer and friction flow characteristics using numerical methods. Poitras *et al.* [6] investigated the flow structure by using a numerical simulation of transverse ribs. Inter-rib spacing and Reynolds number effects were examined. The length of the recirculation zone was significantly influenced by inter-rib space.

5 Measurement of solar air heater performance

Heat transfer is enhanced by artificial roughness at the expense of friction, resulting in turbulent flow within the SAH duct. A highly efficient and economically feasible collector may be designed by enhancing the Nusselt number with the least amount of pressure drop. In this connection, several designs for solar air collectors have been presented that have different configurations of roughness geometry.

5.1 Hydraulic performance

Pressure drop in the SAH duct is used to assess hydraulic performance, which is again linked to the surplus heat, produced by the fan. Frank and Mark [7] defined the friction factor (f) as a dimensionless version of the pressure drop. The hydraulic performance of SAH is determined by the Darcy-Weisbach equation:

$$f = \frac{2(\Delta P)_d D}{4\rho L V^2}\,, \tag{4}$$

where $(\Delta P)_d$ is the pressure drop in the duct ρ is the density of a fluid, L is the length of the duct and V is the mean fluid velocity.

5.2 Thermal performance

This term refers to the heat transfer from the collector to the circulating air. Thermal performance is determined in terms of the energy gained by the air, solar energy gained by the collector, and the energy lost to the surroundings. Hottel and Woertz [8] presented the following energy equation:

$$q_u = I\tau\alpha - U_L\left(T_p - T_a\right), \tag{5}$$

where T_p and T_a are the plate temperature and ambient temperature, respectively, and U_L is the overall heat loss coefficient which is expressed by the following summation:

$$U_L = U_e + U_t + U_b\,, \tag{6}$$

where U_t is the heat transfer coefficient on the top side, U_b is the heat transfer coefficient on the bottom side, and U_e is the heat loss coefficient on the side surface.

The actual excess heat, transmitted to the air from the SAH duct is calculated using the Hottel–Whillier-Bliss [8] equation

$$q_u = F_R\left[I\tau\alpha - L_f\left(T_i - T_a\right)\right], \tag{7}$$

where L_f is the final length of the duct.

5.2.1 Heat removal factor

When the fluid inlet temperature remains as per the collector temperature, the heat removal factor is defined as the ratio of the actual heat transfer to the maximum possible heat transfer by means of the collector plate

$$F_R = \frac{m^0\,C_p}{A_p U_L}\left[\exp\left(\frac{A_p U_L F_p}{m^0 C_p}\right) - 1\right], \tag{8}$$

where C_p is the specific heat of a fluid, m^0 is the mass flow rate of a fluid, F_p is the collector efficiency factor, and A_p is the surface area of the absorber plate.

The thermal efficiency of a solar collector (η) is defined as

$$\eta = \frac{q_u}{I}. \tag{9}$$

Thermal efficiency can also be expressed by means of Hottel-Whillier-Bliss equation [8]

$$\eta = F_R\left[\frac{I\pi\alpha - U_L\left(T_o - T_a\right)}{I}\right]. \tag{10}$$

Bondi presented the following collector efficiency equation when the air inlet temperature and the surrounding temperature are equal [9]:

$$\eta = F_o\left[\tau\alpha - U_L\frac{T_{fo} - T_{fi}}{I}\right], \tag{11}$$

where T_{fo} and T_{fi} is the fluid outlet and inlet temperature, respectively.

Here F_o is the heat removal factor based on the temperature of the exit air which takes the form

$$F_o = \frac{GC_p}{U}\left[\exp\left(\frac{F'U_L}{GC_p}\right) - 1\right], \tag{12}$$

where G is the function of heat transfer (Eq. (13)), U is the overall heat transfer coefficient and the plate collector efficiency factor F' is the ratio of the actual and the ideal heat absorption in a SAH when the fluid temperature and the collector temperature are equal.

5.3 Thermo-hydraulic performance

The objective of this comparison is to determine the performance of the roughened SAH ducts with smooth SAH ducts. Lewis proves that roughened duct provides better thermo-hydraulic performance (THP) which is defined as the ratio of actual heat transfer to the maximum possible heat transfer under the same pumping power, in accordance with the formula [10]

$$\mathrm{THP} = \frac{\frac{\mathrm{Nu}}{\mathrm{Nu}_s}}{\left(\frac{fr}{fs}\right)^{\frac{1}{3}}}, \tag{13}$$

where Nu and Nu_s are the Nusselt numbers of rough and smooth ducts, respectively, and f_r and f_s are the friction factors of rough and smooth surfaces, respectively. Thermo-hydraulic performance thus indicates the effectiveness of SAH because it includes the pumping power losses due to pressure drop inside the duct.

6 Influence of roughness design on the flow pattern

Artificial roughness geometry can take up various forms and orientations. Rib pitch, rib height, inclination, cross-section of rib, and flow parameters, including Reynolds number, are among the major geometrical variables, which are used to indicate the artificial roughness geometry. The impact of these variables on the THP of the SAH ducts has been examined.

6.1 Influence of relative rib pitch

Prasad and Saini [11] explained the influence of the ratio of the pitch to the rib height (P/e) on the flow variation. If the P/e ratio is between 8 to

10, then the reattachment point becomes higher and the heat transfer can be the maximum. Conversely, if the P/e ratio is less than 8, then the flow deviates. If this ratio is beyond 10, it decreases the reattachment point and reduces the heat transfer rate.

6.2 Influence of relative rib height

Prasad and Saini [12] also explained how the height of rib roughness influences flow variation. In this context, the authors explained its effect on the SAH duct. While the rib height can cause the separation of flow and reattachment, the area close to the reattachment ensures the most efficient heat transfer. Reattachment occurs when the e/D is only moderate, as seen in Fig. 2.

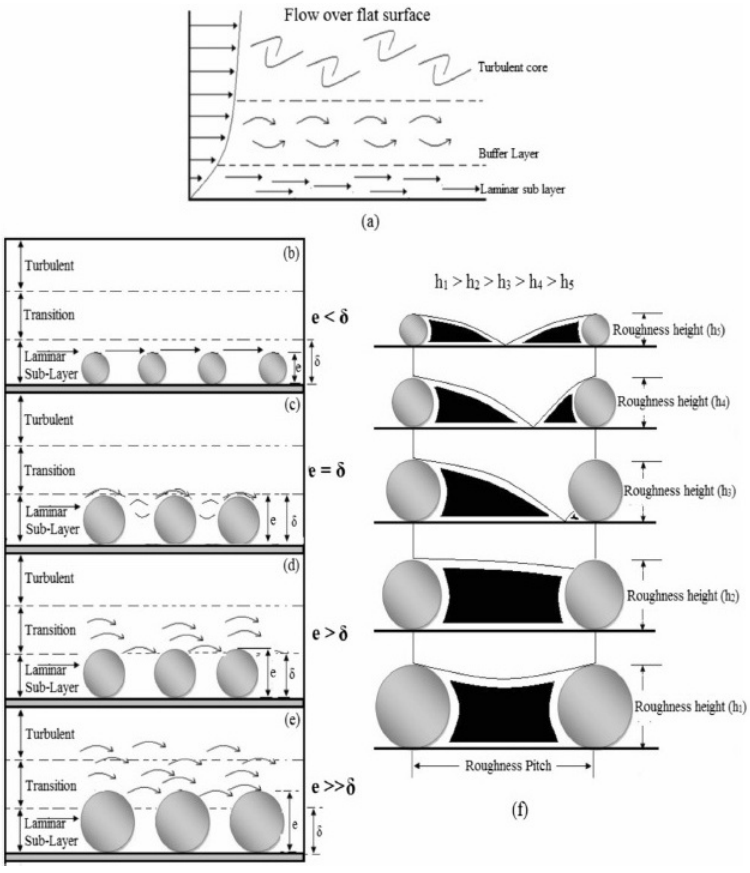

Figure 2: Influence of relative rib height (δ denotes the laminar sublayer height) [12].

6.3 Influence of rib inclination

The angle at which the rib element is aligned in relation to the flow direction is an essential factor behind the counter-revolving secondary flow throughout the span, determining variable heat discharge rates. When fluid comes out from the leading edge and goes to the trailing edge, it is trapped and its temperature goes up. It has been observed that no turbulence, created by transverse ribs, reduces the heat transfer rate because of the rise in fluid temperature at the wall. When the angle in the rib geometry alters, turbulence is created, thereby enhancing the heat transfer rate. Therefore, it is always beneficial for the rib geometry to have a degree of inclination. The heat transfer is maximum at the leading edge and it reduces when it goes to the trailing edge, as shown in Fig. 3.

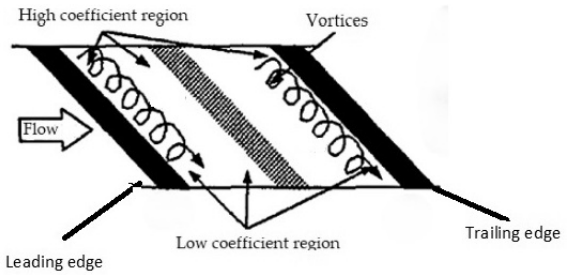

Figure 3: Flow pattern due to angled rib [13].

6.4 Influence of duct aspect ratio

The ratio of the width to height of the duct (W/H) is known as the aspect ratio, which considerably impacts the thermal performance of the SAH. With a moderate increase in the heat discharge, a high duct aspect ratio enhances turbulence inside the duct and raises the friction factor. On the other hand, with a minimum height-to-width ratio, SAH exhibits better heat convective performance. The flow is faster in the duct because the cross-sectional area is shorter. Hence, it increases the heat transfer rate of the flowing fluid. A number of researches have been undertaken to find out the parameters for the optimal width and height of a duct to achieve the optimum heat transfer.

6.5 Influence of relative gap position

A secondary heat flow is released by creating a space in continuous ribs. Afterwards, the main heat flow along with the secondary flow passes through the gap and the flow. As a result, the thermal barrier layer weakens, resulting in a greater heat transfer coefficient. On the one hand, a small gap cannot offer enough area for adequate heat flow. On the other hand, if there is a large gap, the flow is retarded [14]. Hence, the gap should have the optimal width for attaining the best heat transfer coefficient.

6.6 Influence of relative roughness width

The relative roughness width (W/w) pertains to the total width of the absorber plate (W). For understanding the concept, one can consider attaching a rib to the absorber plate in a V-shape, with two of its edges at the leading sections and a third one at the trailing section. One would observe that in comparison to the trailing edge, the heat transfer rate is higher at the leading edges. It is due to the turbulent nature of the fluid at the leading edges that the heat transfer rate is higher there. When the flow moves into the trailing edge, it becomes almost stagnant, reducing the heat transfer rate [15]. It has been established that when W/w rises from 1 to 6, the rate of heat transfer improves. The peak is at 6 after which it declines.

7 Artificial roughness patterns in the solar air heater

During the present study, various rib arrangements that influence friction and heat transfer properties were examined. The following sections focus on the effects of different patterns of roughened surfaces as observed in SAH ducts.

7.1 Transverse rib

7.1.1 Continuous transverse rib

The solar air heater, designed by Prasad and Saini [16], made use of wires with small diameters for ensuring roughness. As part of their experiments, the authors increased the P/e ratio from 10 to 20 while changing the e/D

ratio from 0.02 to 0.033. Following their experiment, Prasad and Saini found the maximum increase in Nu and f by 2.38 and 4.25 times, respectively, at the P/e of 10.

Verma and Prasad [17] examined the Nu and f in circular wire ribs with fixed geometrical parameters. Their experiments revealed the e/D ratio varying from 0.01 to 0.03, the P/e ratio varying from 10 to 40, Re^{+} varying between 8 and 42, and Re ranging between 5000 and 20000. Furthermore, the maximum THP of 71% was recorded at a roughness Reynolds number of 24.

The impact of transverse wire, attached to the absorber plate, as well as the effect of heat transfer and friction on the transition flow regime, were examined by Gupta *et al.* [18]. The Reynolds number is, in fact, a function of the Stanton number. The St rises when Re increases and it reaches its maximum value when Re reaches 12 000.

7.2 Transverse broken ribs

Sahu and Bhagoria [19] investigated Nu and f for broken transverse ribs with fixed geometrical parameters. Their study involved four parameters, including the P/e ratio varying from 10 to 30, e/D ratio of 1.5, aspect ratio (W/H) of 8, and Re ranging from 3000 to 12 000. Their experiments established that the optimum range of the Nusselt number could be attained when the pitch was at $P = 20$ mm. The maximum enhancement of the heat transfer coefficient by 1.25 to 1.4 times as compared to the smooth plate was obtained. Figure 4 depicts the transverse broken rib geometry.

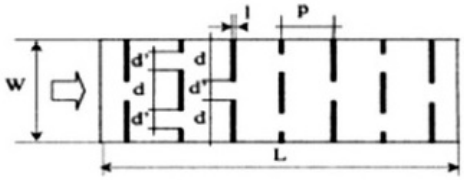

Figure 4: Transverse broken small diameter wire [19].

7.3 Inclined ribs

7.3.1 Continuously inclined ribs

According to Gupta *et al.* [18], inclined ribs are superior to transverse ribs. During experimentation, the authors changed the W/H ratio from 6.8 to

11.5, the e/D value varied from 0.018 to 0.052, the P/e ratio was fixed at 10 and the Re changed from 3000 to 18 000. Following their experimentation, Gupta and his team found the thermal efficiency in the roughened plates to improve by a range of 1.16–1.25 times compared to the smooth plates.

7.3.2 Inclined broken ribs

The impact of a gap in the continuously inclined ribs was examined by Aharwal *et al.* [14]. The different parameters of the continuous inclined ribs included the P/e ratio at 10, the e/D ratio of 0.377, the W/H ratio of 5.84, the angle of attack (α) at 60 deg, and the Re varied from 3000 to 18 000. During experimentations, the gap width of the ribs was also changed from 0.5 to 2 and the relative gap position was altered from 0.16 to 0.67. Accordingly, the maximum enhancements in the Nu and f in ducts with the continuous inclined ribs were recorded at 2.59 and 2.87 that for a flat plate, respectively. Figure 5 depicts the continuous inclined geometry of the ribs. Aharwal *et al.* [20] changed the dimensions and calculated Nu and f. In their study, different parameters were varied, such as the P/e ratio altered from 4 to 10, the e/D ratio changed from 0.018 to 0.0377, and the angle of inclination in flow direction (α) altered from 30 to 90 deg. Aharwal and his team attained the highest Nu and f increased by 2.83 and 3.6 times, respectively, as compared to flat ducts. Thermo-hydraulic performance was reported to be maximum for relative gap width of 1.0 and a relative gap position of 0.25.

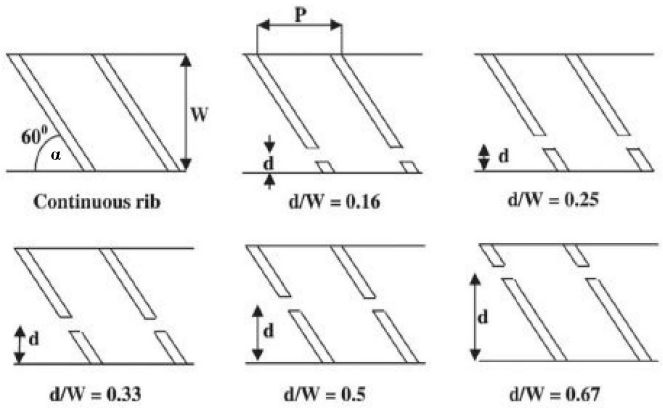

Figure 5: Inclined broken ribs [20].

7.4 V-shape rib

7.4.1 V-shape continuous rib

Momin *et al.* [21] investigated the impact of the V-shaped ribs connected to the absorber plate. During the experiments, the authors varied α from 30 to 90 deg and the e/D ratio from 0.02 to 0.034. Both the Nu and f were enhanced to the maximum at the 60-degree α as compared to a flat duct. In the course of their probe, the authors discovered that the V-shaped ribs performed better than the inclined ribs. The performance of Nu in V-shape rib was 1.14 times the one for the inclined ribs, having equal rib height, pitch, and other operating conditions.

Roughness geometry in V-shaped rib was investigated by Isanto *et al.* [22]. According to their published article, they set the e/Dratio at 0.033, α at 30 to 80 degrees, and P/e at 10. Following their experiments, the f and Nu were recorded to increase 2.45 and 2.34 times, respectively, when compared to the flat plate.

7.4.2 Discrete V-rib

Karwa *et al.* [23] used V- discrete and V- discontinuous ribs in their experiment. The parameters, set by them, were the P/e ratio at 10.63, relative roughness length (B/S, Fig. 6) which is defined as the ratio of the half-length of the V-rib element to the short-way length of the mesh and varied from 3 to 6, and angles of attack set at 45 to 60 deg. The Re value also varied from 2850 to 15 500. The authors observed that discrete ribs outperformed discontinuous ribs and the angle of attack at 60-degree ribs performed better compared to 45-degree ribs. Figure 6 depicts the V-shape's rough geometry.

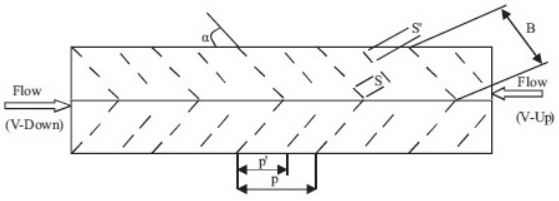

Figure 6: V-shape rib different geometry [23].

Muluwork *et al.* [24] compared the V-down rib, V-up rib, transverse discrete rib, and V-down discrete rib. Studies revealed that the value of St for V-up

and transverse discrete ribs is less than for V-down discrete ribs. Within the range of the parameters studied, the St was found to have a maximum value between 1.32 and 2.47. Karwa [25] examined the V-down continuous, V-up continuous, inclined transverse, V-down discrete, and V-up discrete ribs. He found that the V-down ribs facilitated the maximum heat transfer when pumping powers were equal in both artificially roughened and smooth ducts.

Singh *et al.* [26] investigated the discrete rib with a V-shaped geometry. In their study, the Re values varied from 3000 to 15 000, the relative gap position (g/e) from 0.5 to 2.0, the e/D ratio from 0.015 to 0.043, α varied from 30 to 75 deg and the P/e ratio ranged between 4 and 12. They found that maximum Nu and f increased by 3.04 and 3.11 times, respectively, as compared to smooth plates. Figure 7 depicts the V-down discrete roughness geometry.

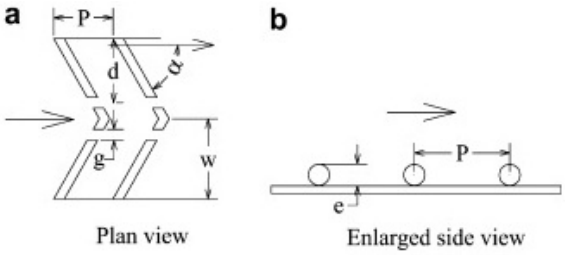

Figure 7: V-down discrete rib [26].

7.5 Ribs with multiple V-shape

7.5.1 Continuous multi V-rib

According to Hans *et al.* [27], the roughness of a variety of V-ribbed ducts is characterized by Reynolds numbers, the e/D and P/e ratios, the angle of inclination, and the W/w value changes from 1 to 10. They observed heat transfer to be the maximum when W/w is equal to 6. The authors pointed out that if the W/w value is less or greater than 6, the extent of heat transfer decreases. Figure 8 depicts the roughness geometry. Maximum enhancement in Nusselt number and friction factor was six- and five-fold, respectively, in comparison to the smooth duct for the range of parameters investigated.

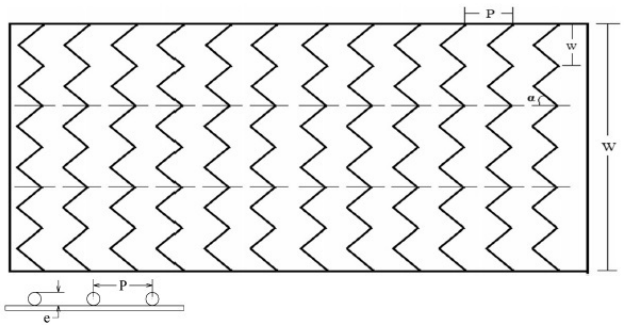

Figure 8: Continuous multi V-rib [27].

7.5.2 Multi V-shaped ribs with a gap

Kumar *et al.* [28] examined the acceleration of heat flow and generation of local turbulence by creating a gap between the V-shaped ribs. Accordingly, the e/D ratio was recorded at 0.043, angles of inclination at 30 to 75 deg, relative roughness pitch at 10, relative gap distance ratios at 0.20 to 0.80, relative gap widths at 0.55 to 1.5, relative width ratio at 6, and Re varied from 2000 to 20 000. The thermo-hydraulic performance (THP) was also found to be significantly boosted compared to a smooth plate. They reported maximum enhancement in Nu and f as 6.32 and 6.12 times that of smooth duct, respectively.

7.6 Arc-shaped ribs

Roughness geometry in an arc-shaped rib was investigated by Saini and Saini [29]. Accordingly, the e/D ratio ranged from 0.0213 to 0.0422, angles of inclination varied from 30 to 75 deg, the P/e value was 10 and Re varied from 2000 to 17 000. The roughness geometry of the arc-shaped ribs improved the Nu to a maximum value of 3.80 and f increased 1.75 times compared to the smooth plate. Figure 9 depicts the arc roughness geometry.

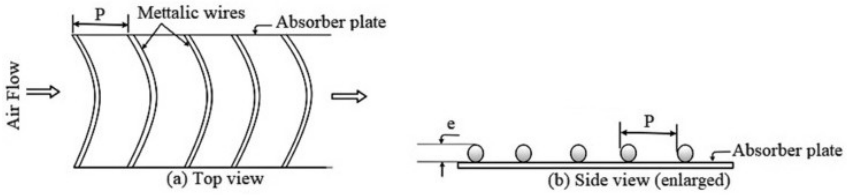

Figure 9: Rib roughness in arc shape [29].

7.7 Multi-arc ribs

Continuous arc multi-rib

Singh *et al.* [30,31] probed the concept of multi-arc roughness. The Reynolds numbers were kept between 2200 and 22 000, the e/D ratio ranged between 0.018 and 0.045, the P/e value varied from 4 and 16, whereas the width ratio was between 1 and 7. They reported maximum enhancement in the Nu and f as 3.71. and 5.07 times that of smooth duct, respectively.

7.7.1 Multiple arc ribs with a gap

Pandey *et al.* [32] studied the concept of multi- arc-shaped roughness geometry with a gap. During the experimentation, e/D varied from 0.016 to 0.044, P/e varied from 4 to 16, the gap width ratio changed from 1 to 7, α varied from 30 to 75 deg, the relative gap varied from 0.5 to 2 and the dimensionless position of the gap ranged from 0.25 to 0.85. The heat transfer on this rough surface is much better than on a smooth one. In fact, it's 5.85 times more effective in moving heat. So, the rough surface is a lot better at transferring heat. Figure 10 depicts the arc roughness geometry.

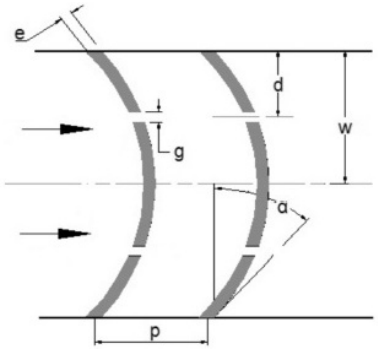

Figure 10: Multiple arc-shaped ribs with gap [32].

7.8 W-shape ribs

The roughened W-shaped SAH duct used by Lanjewar *et al.* [33,34] is shown in Fig. 11. The authors carried out experiments by varying Re from 2000 to 14 000, e/D from 0.018 to 0.03375, angle of inclination from 30 to 75 deg while keeping P/e fixed at 10. They reported maximum enhancement in

Nu as 2.36 times and in friction factor as 2.01 times in comparison to the smooth plate for a 60-degree angle of inclination.

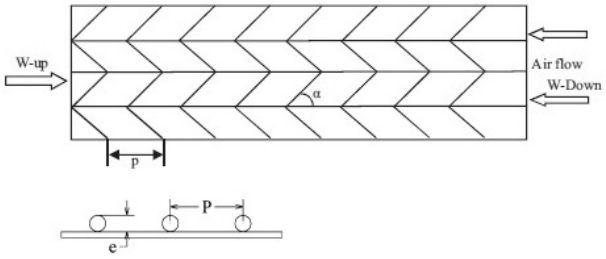

Figure 11: Continuous W-shape rib roughness [33].

7.8.1 Discrete W-shaped rib

Roughness geometry in discrete W-shaped was investigated by Kumar *et al.* [35]. During experimentation, the authors changed e/D from 0.0168 to 0.0338, P/e was fixed at 10, the angle of attack was between 30 to 75 deg, while the Reynolds number varied from 2000 to 15 000. The rise of 2.16 and 2.75 times in Nu and f were observed, respectively, as compared to a flat plate at an angle of inclination of 60 deg.

7.9 Arc-shaped dimple rib

Yadav *et al.* [36] experimented with the arc-shaped dimple coarseness as shown in Fig. 12. During test series, the authors changed different parameters, including e/D, P/e, Reynolds number, and angle of inclination. Yadav and his team found that the thermal efficiency in the roughened plates improves as compared to smooth plates. The friction factor and Nusselt number were increased by 2.93 and 2.89 times with respect to the smooth duct for an angle of attack of 60 deg, a relative pitch of 10, and a relative rib height of 0.03.

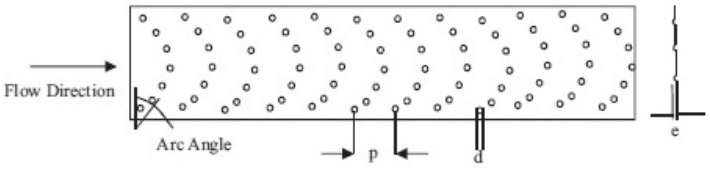

Figure 12: Dimple arc-shaped roughness [36].

Sethi *et al.* [37, 38] examined angular dimple-shaped ribs with different relative pitches and heights. They investigated the geometries with the P/e set from 10 to 20, e/D from 0.021 to 0.036, and arc angles from 45 to 75 deg. The maximum Nu was calculated based on the P/e at 10, e/D at 0.036, and arc angles at 60 deg. They observed an improvement in the thermo-hydraulic performance (THP) of 1.10 to 1.887 times in comparison to the smooth plates.

7.10 Transverse dimple roughness

Saini *et al.* [39] were the first to experiment with artificial roughness created by means of dimpled ribs instead of transverse ribs. During experimentation, the authors changed various parameters like e/D and P/e ratios, and Reynolds numbers. Saini and his team also determined the maximum Nu and f value for P/e at 10. They reported the maximum value of the Nusselt number for a relative roughness height of 0.0379 and a relative roughness pitch of 10.

7.11 Staggered dimple roughness

Bhushan *et al.* [40] experimented with the staggered dimpled roughness instead of the transverse-shaped dimpled roughness. In their study, the duct aspect ratio was 10 while the relative print diameter ranged from 0.147 to 0.367, the relative long-way length (L/e) 25 was set at 37.50 and the relative short-way length (S/e) ranged from 18.75 to 37.5. The maximum enhancement of the Nusselt number and friction factor was increased by 3.8 and 2.2 times, respectively, as compared to the smooth plates. Figure 13 depicts the staggered dimple roughness geometry.

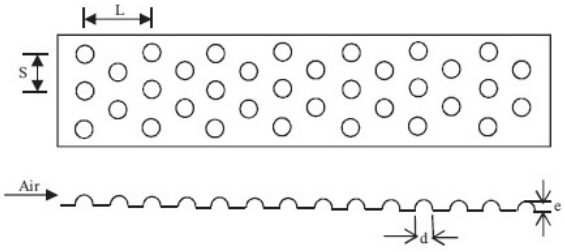

Figure 13: Staggered dimple rib roughness [40].

7.12 Wedge-shaped ribs

According to Bhagoria *et al.* [41] the SAH heat flow and flow characteristics can be improved by roughening the absorber plates and by incorporating transverse ribs, as shown in Fig. 14. In their experiment, the rib wedge angle (Φ) ranged from 8 to 15 deg, e/D from 0.015 to 0.033 and the Reynolds number from 3000 to 18 000. When the difference between the rough and flat plates is compared, the Nu and f were increased by 2.4 and 5.3 times, respectively, in comparison to the flat plates following this experiment.

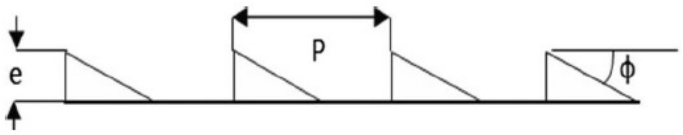

Figure 14: Wedge rib roughness [41].

7.13 Chamfered ribs

The artificial chamfered rib roughness, as shown in Fig. 15, was analyzed by Karwa *et al.* [42]. In their experiment, the relative roughness pitch varied between 4.5 and 8.5, the roughness height within 0.0141–0.0328, the duct aspect ratio ranged from 4.8 to 12, the rib chamfer angles from 15 to 18 deg, and the Reynolds numbers varied between 3000 and 20 000. They observed an improved THP in plates having chamfered-shaped ribs as compared to the smooth plate. The maximum enhancement factor in friction factor and Nusselt number were found to be 3.74 and 3.24, respectively.

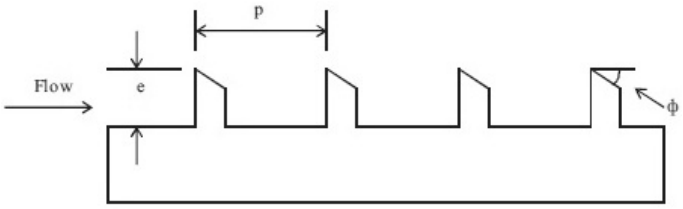

Figure 15: Chamfered ribs [42].

7.14 Combination of ribs

Varun *et al.* [43] investigated the effects of combined inclined and transverse ribs. The researchers modified some parameters, such as P/e, e/D, and

Reynolds number, and tried with a fixed ratio of the duct aspect ratio. The geometry having a relative roughness pitch of 8 had the maximum thermal efficiency. Layek *et al.* [44] investigated the effects of chamfer grooved ribs. They experimented with the e/D ratio ranging from 0.022 to 0.04, P/e from 0.3 to 0.6, relative groove position (g/P) from 0.3 to 0.6, as well as the chamfered angles of 50 to 30 degrees. They found the maximum thermal performance by keeping the relative groove position at 0.4.

Ravi and Saini [45] studied the multi-V-shaped gap with staggered ribs by using different operating parameters, as shown in Fig. 16. They varied the staggered rib pitch (p/P) from 0.2 to 0.8, the staggered rib ratio (r/e, where r is the staggered rib length) between 1 and 4 and kept the W/w ratio at 8. The authors achieved the maximum augmentation of heat transfer at p/P of 0.6, r/e of 3.5, and W/w equaling 8. In another work, Ravi and Saini [46] investigated the double-pass (DP) SAH, having a multi V-shaped gap with staggered ribs. The analysis included parameters such as p/P varied from 0.2 to 0.8, r/e ratio between 1 and 4, and W/w values from 5 to 8. At the corresponding values of p/P amounting to 0.6, r/e ratio of 3.5, and W/w of 7, they found the maximum thermo-hydraulic performance (THP) parameter as compared to the smooth plates.

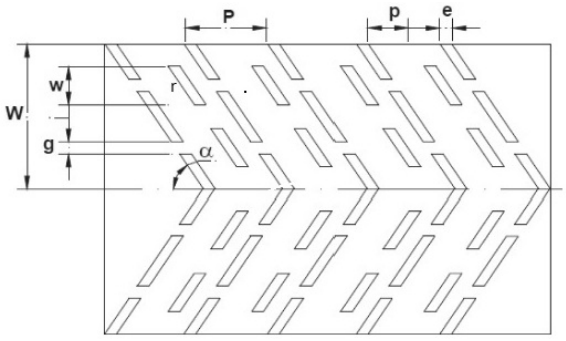

Figure 16: Multi-V-shaped discrete and staggered rib [45, 46].

The performance of the V-shaped discrete and staggered rib was analyzed by Patel and Lanjewar [47], as shown in Fig 17. The maximum value of Nu and f were found to be 2.27 and 4.28 times that of a flat plate, respectively.

Patel and Lanjewar [48] experimented with symmetrical V-shaped gaps and staggered ribs in the duct to evaluate their influence on SAH. They found that the number of gaps in the ribs affects the performance of SAH. At the number of gaps of 3, the authors attained the maximum rise of

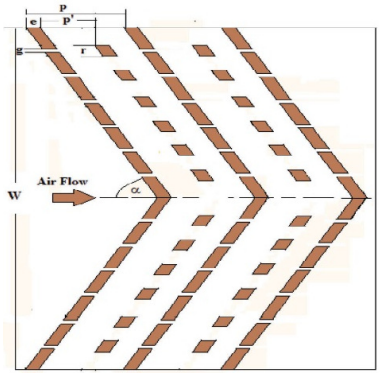

Figure 17: Multiple V-shaped discrete combined with staggered ribs [47].

2.05 and 3.39 times, respectively, in the Nu and f as compared to a flat plate. They also found the maximum THP value of 1.59 as compared to the smooth plate when the number of gaps was 3. Figure 18 depicts the symmetrical V-shaped gap and staggered rib roughness geometry.

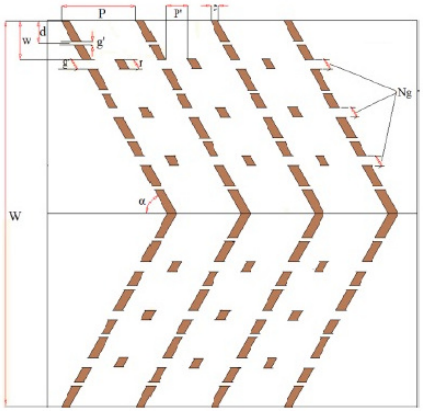

Figure 18: Symmetrical V-shaped gap and staggered rib roughness [48].

In their study, Patel and Lanjewar [49] also observed that the relative roughness pitch P/e varied while other parameters, including e/D, relative gap position (g/e), dimensionless gap width (d/W), p'/P, r/e and the number of gaps, remained constant. They found the maximum value of Nu at P/e of 10.

A novel V-rib symmetrical gap and staggered rib element in a SAH were examined by Jain and Lanjewar [50]. They found how artificial roughness

affects the SAH performance, as shown in Fig. 19. They found the maximum value of the THP parameter at $P/e = 12$.

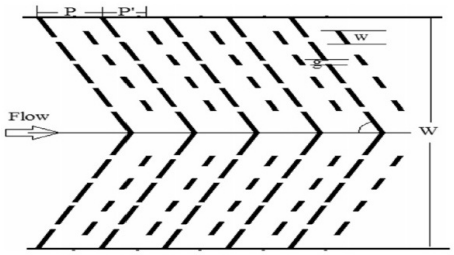

Figure 19: V-rib symmetrical gap with staggered element rib [52].

Patil *et al.* [51–53] investigated a SAH plate with V-rib gaps combined with staggered elements, as shown in Fig. 20. The relative gap positions were changed from 0.2 to 0.8 while all other parameters, including e/D, P/e, relative staggered rib size, and the staggered rib location, remained unchanged. They noted an enhancement in the hydraulic performance varying from 1.48 to 2.10 times and a rise in the Nusselt number from 1.89 to 2.85 times that of the smooth plate.

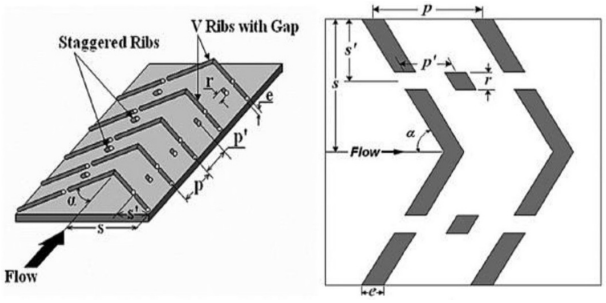

Figure 20: Combination of V-rib gaps with staggered element rib [51–53].

Similarly, Deo *et al.* [54] experimented with V-rib gaps combined with the staggered element. Several parameters were altered, including the relative roughness diameter (e/D) of 0.065, the relative pitch of ribs (P/e) from 4 to 14, the angle of attack from 40 to 80 deg, the number of gaps per limb fixed at 2, relative staggered rib size (r/e) of 4.5 and relative gap width (w/e) of 1. They found the maximum thermal performance as compared to the flat plate.

7.15 Wire mesh

7.15.1 Expanded metal mesh

Saini *et al.* [55] focused on the expanded metal mesh roughness geometry, as shown in Fig. 21. First, they combined relative long way length (L/e) and relative short way length (s/e). They also studied the effects of friction and heat transfer. Their experiments revealed heat transfer coefficients and friction factors rising 4 and 5 times, respectively, as compared to the flat plate.

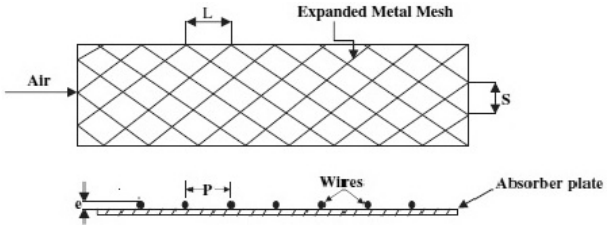

Figure 21: Expanded metal mesh [55].

7.15.2 Discrete metal mesh

Karmare and Tikekar [56] investigated discrete metal mesh, as illustrated in Fig. 22. The authors studied a number of parameters, such as e/D, P/e, Reynolds number and metal grid dimensions. They discovered that plates with roughness values of $e/D = 0.044$, $l/s = 1.72$, and $P/e = 17.5$ performed best.

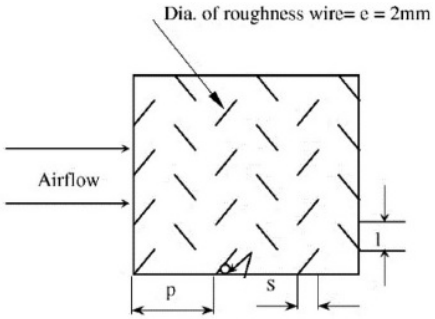

Figure 22: Metal grid rib roughness [56].

7.16 Other roughness

7.16.1 W-rib roughness geometry

Thakur and Thakur [57] investigated W-shaped rib geometry. They experimented with a unique roughness geometry. During the investigation, they altered several parameters, such as the relative staggered length (w/e), relative staggered pitch (p/P), e/D, α, P/e, Re and number of gaps. With the experiment, Thakur and his team could enhance the Nu and f by 3.3 and 4.1 times as compared to smooth ducts, respectively.

Kumar *et al.* [58] examined the effect of an S-shaped configuration on the arc ribs. The parameters used by the team included the e/D was 0.022, W/w varying from 1-4 to 0.054, the P/e varying from 4 to 16, and the angle of attack (α) fixed at 60 deg. Kumar and his team could enhance the Nusselt number 2.71 times and friction factor 4.64 times, as compared to smooth ducts.

7.16.2 Combination of the arc with gap shape and staggered piece

Gill *et al.* [59] investigated a SAH with a broken arc paired with staggered rib roughness geometry. The authors conducted experiments to investigate the impact of different coarseness parameters on Nu and f, including P/e, r/g, e/D, W/w, and relative staggered rib position (P'/P). Figure 23 depicts the roughness geometry. The maximum obtained enhancement of Nusselt number and friction factor was 2.04 and 4.18 times that of a flat plate, respectively.

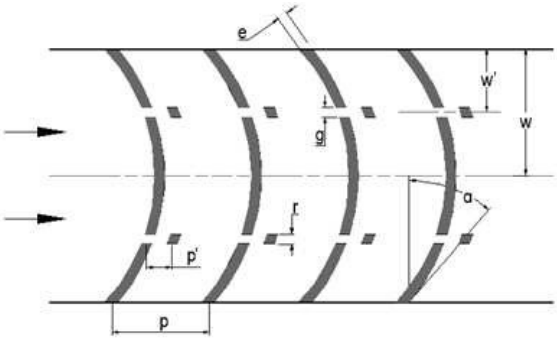

Figure 23: Combination of broken arc rib with staggered rib [59].

7.16.3 A symmetrical arc with multiple gaps:

Jain *et al.* [60–62] investigated arc shape geometry using various gaps in a single arc. The parameters, used in their study, were the Reynolds number between 3000 and 18 000, relative roughness pitch (P/e) at 12, arc angle (α) at 60 deg, g/e varying from 2 to 5, and e/D of 0.047. With the experiment, Jain and his team could enhance the Nusselt number 2.77 times and the friction factor 3.66 times, as compared to flat ducts.

8 Thermo-hydraulic effectiveness of artificial roughened surfaces

To sum up, a significant rise in the friction factor was observed with the incorporation of artificial coarseness in order to improve heat transfer. Hence, roughness geometry proved to be essential for heat transfer to a greater degree while minimizing friction losses. While choosing the methods for enhancement of heat transfer, one has to account for the huge requirement of pumping energy as turbulence in the flow results in a significant pressure drop. A high rate of heat transfer at the minimum pumping energy is essential for developing an effective and compact SAH.

During the present study, the Nusselt number and the friction factor values for the roughened and smooth absorber surfaces were compared using the parameters for thermo-hydraulic performance (THP). Figure 24 represents the friction factor *versus* the Reynolds number and shows that an increase in the Reynolds number results in a friction factor decrease. According to Fig. 24, the optimal outcome for the friction factor along the whole range of the Reynolds number is not a single geometry. The maximum value of friction factor is obtained in the case of continuous multi V-rib geometry.

They were also compared with their respective Reynolds numbers, as shown in Fig. 25. The THP characteristics with a wide array of values, ranging from 0.49 to 3.70, are presented in Fig. 25. The THP parameter is the lowest when the inclined angle and transverse ribs are combined. However, multiple V-ribs with a gap ensure the highest rate of heat transfer. At low Reynolds numbers, multi-arc ribs with gaps are not very effective. However, their performance improves dramatically as the Reynolds number increases.

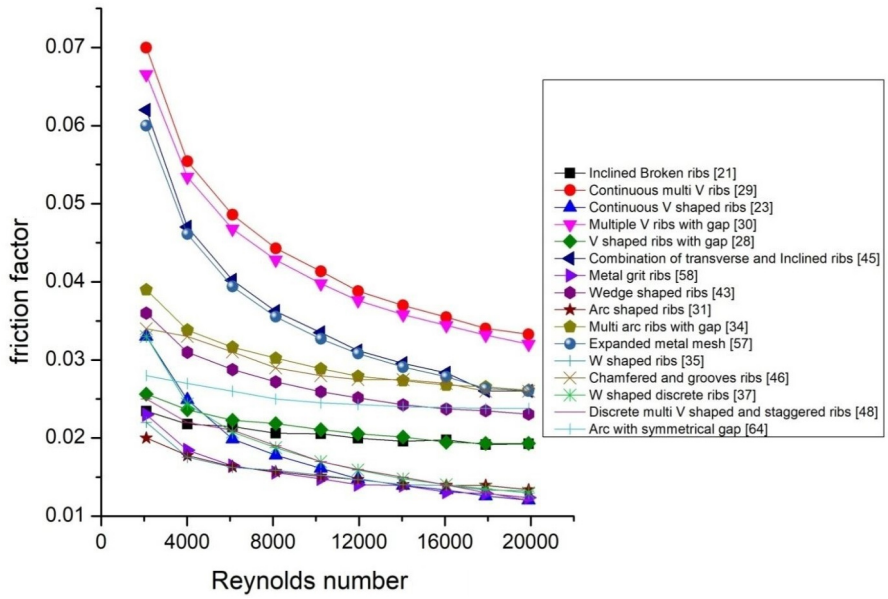

Figure 24: Friction factor with respect to Reynolds number, based on data from different research works.

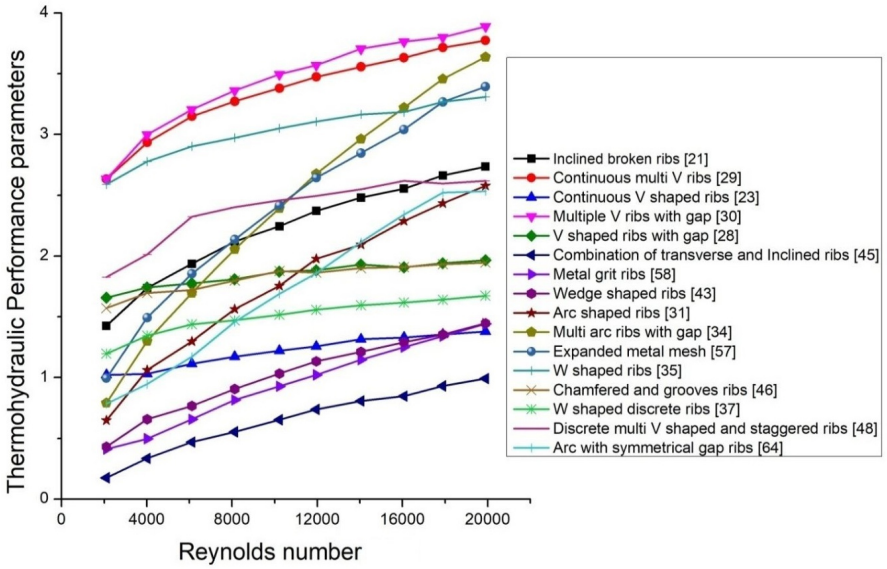

Figure 25: Comparison of thermo-hydraulic performance parameters for various roughened surfaces determined based on data reported by different researchers.

9 Conclusions

The present study has attempted a thorough examination of several artificial roughness configurations in solar air heaters as suggested by a number of researchers. The impact of different shapes of coarseness and flow characteristics on heat transfer and friction factors has also been discussed. The following conclusions may be taken from the data that has been analyzed.

1. Artificial coarseness in the form of small ribs on the undersurface of the absorber plate is an excellent alternative for improving heat transfer in solar air heaters. However, at the same time, artificial roughness is responsible for the increased friction factor which enhances the demand for pumping power.

2. The characteristics of various parameters such as relative roughness pitch, relative roughness height, angle of attack, and rib arrangement, i.e. inclined, transverse, single V-shape, multiple V-shape, arc-shape, and multi arc-shape ribs were investigated.

3. For almost the entire experimental setup, the maximum values of the Nusselt number and friction factor were obtained for the relative roughness pitch (P/e) of 8 to 10, the relative roughness height (e/D) of 0.03, and an angle of attack (α) of 60 deg.

4. Compared to continuous ribs, insertion of V-gaps in continuous ribs, continuous arc ribs, and continuous W-ribs enhance the friction factor and heat transfer rate.

5. The maximum increase in heat transfer was recorded for multiple V-rib geometry with a gap, followed by multiple V-shaped rib geometry and multiple arc-shaped rib geometry with a gap. Due to providing a gap in continuous V-ribs, multi V-ribs, arc ribs, and multi arc-ribs, the Nusselt numbers were increased by 1.32,1.12,1.33, and 1.15 times, respectively.

6. Continuous multiple V-rib geometry showed a significant increase in the friction factor, followed by multiple V-rib geometry with a gap.

7. S-shaped ribs, metal rib grids, and ribs with grooves proved to be inadequate. Each of these types needed machining in order to create grooves.

8. Comparison of the-hydraulic performance parameter with respect to the Reynolds number has been performed. Maximum of thermo-hydraulic performance were found for W-ribs, multiple V-ribs with a gap, and multiple arc-rib with a gap in different Reynolds number.

This review article will assist researchers in understanding the importance of the roughness aspect that significantly increases the the Nusselt number and friction factor, thereby improving the operation of solar air heaters. Accordingly, one could work on the development of designs for alternative configurations of rectangular solar air heater ducts by using these roughness factors.

Received 22 October 2022

References

[1] Tiwari G.N.: *Solar Energy: Fundamentals, Design, Modelling and Applications*. Alpha Sci., 2002.

[2] Gawande V.B., Dhoble A.S., Zodpe D.B., Chamoli S.: *A review of CFD methodology used in literature for predicting thermo-hydraulic performance of a roughened solar air heater*. Renew. Sustain. Energy Rev. **54**(2016), 550–605.

[3] Bhatti M.S., Shah R.: *Turbulent and transition flow convective heat transfer in ducts*. In: Handbook of Single-Phase Convective Heat Transfer (S. Kakaç, R.K. Shah, W. Aung, Eds.). Wiley, New York 1987.

[4] Nikuradse J.: *Laws of Flow in Rough Pipes*. NACA TM 1292, Washington 1950.

[5] Dipprey D.F., Sabersky R.H.: *Heat and momentum transfer in smooth and rough tubes at various Prandtl numbers*. Int. J. Heat Mass Transf. **6**(1963), 5, 329–353.

[6] Poitras G.J., Brizzi L.E., Gagnon Y.: *Structure of channel flows with surface mounted ribs*. J. Therm. Sci. **13**(2004), 3, 213–219.

[7] Kreith F., Bohn M.S.: *Principles of Heat Transfer*. Thomson Learning, 2001.

[8] Hottel H.C., Bernard B.W.: *The performance of flat-plate solar heat collectors*. In: Renewable Energy (Bent Sorensen, Ed.). Taylor & Francis, Routledge 2018, 324–355.

[9] Biondi P., Cicala L., Farina G.: *Performance analysis of solar air heaters of conventional design*. Sol. Energy **41**(1988), 1, 101–107.

[10] Lewis M.J.: *Optimising the thermohydraulic performance of rough surfaces*. Int. J. Heat Mass Transf. **18**(1975), 11, 1243–1248.

[11] Prasad B.N., Saini J.S.: *Optimal thermohydraulic performance of artificially roughened solar air heaters*. Sol. Energy **47**(1991), 2, 91–96.

[12] Prasad, B.N., Saini J.S.: *Effect of artificial roughness on heat transfer and friction factor in a solar air heater*. Sol. Energy **41**(1988), 6, 555–560.

[13] Taslim M.E., Li T., Kercher D.M.: *Experimental heat transfer and friction in channels roughened with angled, V-shaped, and discrete ribs on two opposite walls*. J. Turbomach. **118**(1996), 1, 94-GT-163, V004T09A018.

[14] Aharwal K.R., Gandhi B. K., Saini J.S.: *Experimental investigation on heat-transfer enhancement due to a gap in an inclined continuous rib arrangement in a rectangular duct of solar air heater*. Renew. Energy **33**(2008), 4, 585–596.

[15] Kumar A., Kim M.-H.: *CFD analysis on the thermal hydraulic performance of an SAH duct with multi V-shape roughened ribs*. Energies **9**(2016), 6, 415.

[16] Prasad B.N., Saini J.S.: *Effect of artificial roughness on heat transfer and friction factor in a solar air heater*. Sol. Energy **41**(1988), 6, 555–560.

[17] Verma S.K., Prasad B.N.: *Investigation for the optimal thermohydraulic performance of artificially roughened solar air heaters*. Renew. Energy **20**(2000), 1, 19–36.

[18] Gupta D., Solanki S.C., Saini J.S.: *Heat and fluid flow in rectangular solar air heater ducts having transverse rib roughness on absorber plates*. Sol. Energy **51**(1993), 1, 31–37.

[19] Sahu M.M., Bhagoria J.L.: *Augmentation of heat transfer coefficient by using 90 broken transverse ribs on absorber plate of solar air heater*. Renew. Energy **30**(2005), 13, 2057–2073.

[20] Aharwal K.R., Gandhi B.K., Saini J.S.: *Heat transfer and friction characteristics of solar air heater ducts having integral inclined discrete ribs on absorber plate*. Int. J. Heat Mass Transf. **52**(2009), 25-26, 5970–5977.

[21] Momin A.-M.E., Saini J.S., Solanki S.C.: *Heat transfer and friction in solar air heater duct with V-shaped rib roughness on absorber plate*. Int. J. Heat Mass Transf. **45**(2002), 16, 3383–3396.

[22] Istanto T., Danardono D., Yaningsih I., Wijayanta A.T.: *Experimental study of heat transfer enhancement in solar air heater with different angle of attack of V-down continuous ribs*. AIP Conf. Proc., **1737**(2016), 1, 060002.

[23] Karwa R., Bairwa R.D., Jain B.P., Karwa N.: *Experimental study of the effects of rib angle and discretization on heat transfer and friction in an asymmetrically heated rectangular duct*. J. Enhanc. Heat Transf. **12**(2005), 4, 343–355.

[24] Muluwork K.B., Saini J.S., Solanki S.C.: *Studies on discrete rib roughened solar air heaters*. In: Proc. National Solar Energy Convention-98, Roorkee SESI **75**(1998), 84.

[25] Karwa R: *Experimental studies of augmented heat transfer and friction in asymmetrically heated rectangular ducts with ribs on the heated wall in transverse, inclined, V-continuous and V-discrete pattern*. Int. Commun. Heat Mass Transf. **30**(2003), 2, 241–250.

[26] Singh S., Chander S., Saini J.S.: *Heat transfer and friction factor correlations of solar air heater ducts artificially roughened with discrete V-down ribs*. Energy **36**(2011), 8, 5053–5064.

[27] Hans V.S., Saini R.P., Saini J.S.: *Heat transfer and friction factor correlations for a solar air heater duct roughened artificially with multiple v-ribs*. Sol. Energy **84**(2010), 6, 898–911.

[28] Kumar A., Saini R.P., Saini J.S.: *Experimental investigation on heat transfer and fluid flow characteristics of air flow in a rectangular duct with Multi V-shaped rib with gap roughness on the heated plate*. Sol. Energy **86**(2012), 6, 1733–1749.

[29] Saini S.K., Saini R.P.: *Development of correlations for Nusselt number and friction factor for solar air heater with roughened duct having arc-shaped wire as artificial roughness*. Sol. Energy **82**(2008), 12, 1118–1130.

[30] Singh A.P.: *Effect of artificial roughness on heat transfer and friction characteristics having multiple arc shaped roughness element on the absorber plate*. Sol. Energy **105**(2014), 479–493.

[31] Singh A.P.: *Heat transfer and friction factor correlations for multiple arc shape roughness elements on the absorber plate used in solar air heaters*. Exp. Therm. Fluid Sci. **54**(2014), 117–126.

[32] Pandey N.K., Bajpai V.K.: *Experimental investigation of heat transfer augmentation using multiple arcs with gap on absorber plate of solar air heater*. Sol. Energy **134**(2016), 314–326.

[33] Lanjewar A., Bhagoria J.L., Sarviya R.M.: *Heat transfer and friction in solar air heater duct with W-shaped rib roughness on absorber plate*. Energy **36**(2011), 7, 4531–4541.

[34] Lanjewar A., Bhagoria J.L., Sarviya R.M.: *Experimental study of augmented heat transfer and friction in solar air heater with different orientations of W-rib roughness*. Exp. Therm. Fluid Sci. **35**(2011), 6, 986–995.

[35] Kumar A., Bhagoria J.L., Sarviya R.M.: *Heat transfer and friction correlations for artificially roughened solar air heater duct with discrete W-shaped ribs*. Energy Convers. Manage. **50**(2009), 8, 2106–2117.

[36] Yadav S., Kaushal M.: *Nusselt number and friction factor correlations for solar air heater duct having protrusions as roughness elements on absorber plate*. Exp. Therm. Fluid Sci. **44**(2013), 34–41.

[37] Sethi M., Thakur N.S., Varun: *Heat transfer and friction characteristics of dimple-shaped roughness element arranged in angular fashion (arc) on the absorber plate of solar air heater*. J. Renew. Sustain. Energy **4**(2012), 2, 023112.

[38] Sethi M., Thakur N.S.: *Correlations for solar air heater duct with dimpled shape roughness elements on absorber plate*. Sol. Energy **86**(2012), 9, 2852–2861.

[39] Saini R.P., Verma J.: *Heat transfer and friction factor correlations for a duct having dimple-shape artificial roughness for solar air heaters*. Energy **33**(2008), 8, 1277–1287.

[40] Bhushan B., Singh R.: *Nusselt number and friction factor correlations for solar air heater duct having artificially roughened absorber plate*. Sol. Energy **85**(2011), 5, 1109–1118.

[41] Bhagoria J. L., Saini J.S., Solanki S.C.: *Heat transfer coefficient and friction factor correlations for rectangular solar air heater duct having transverse wedge shaped rib roughness on the absorber plate*. Renew. Energy **25**(2002), 3, 341–369.

[42] Karwa R., Solanki S.C., Saini, J.S.: *Heat transfer coefficient and friction factor correlations for the transitional flow regime in rib-roughened rectangular ducts*. Int. J. Heat Mass Transf. **42**(1999), 9, 1597–1615.

[43] Varun, Saini R.P., Singal S.K.: *Investigation of thermal performance of solar air heater having roughness elements as a combination of inclined and transverse ribs on the absorber plate*. Renew. Energy **33**(2008), 6, 1398–1405.

[44] Layek A., Saini J.S., Solanki S.C.: *Heat transfer and friction characteristics for artificially roughened ducts with compound turbulators*. Int. J. Heat Mass Transf. **50**(2007), 23-24, 4845–4854.

[45] Ravi R.K., Saini R.P.: *Effect of roughness elements on thermal and thermohydraulic performance of double pass solar air heater duct having discrete multi V-shaped and staggered rib roughness on both sides of the absorber plate*. Exp. Heat Transf. **31**(2018), 1, 47–67.

[46] Ravi R.K., Saini R.P.. *Nusselt number and friction factor correlations for forced convective type counter flow solar air heater having discrete multi V shaped and staggered rib roughness on both sides of the absorber plate*. Appl. Therm. Eng. **129**(2018), 735–746.

[47] Patel S.S., Lanjewar A.: *Experimental analysis for augmentation of heat transfer in multiple discrete V-patterns combined with staggered ribs solar air heater*. Renew. Energy Focus **25**(2018), 31–39.

[48] Patel S.S., Lanjewar A.: *Performance study of solar air heater duct with gap in V-rib with symmetrical gap and staggered ribs*. Heat Mass Transf. **55**(2019), 9, 2517–2532.

[49] Patel S.S., Lanjewar A.: *Experimental and numerical investigation of solar air heater with novel V-rib geometry*. J. Energy Storage **21**(2019), 750–764.

[50] Jain P.K., Lanjewar A.: *Overview of V-rib geometries in solar air heater and performance evaluation of a new V-rib geometry*. Renew. Energy **133**(2019), 77–90.

[51] Patil A.K., Saini J.S., Kumar K.: *Effect of gap position in broken V-rib roughness combined with staggered rib on thermohydraulic performance of solar air heater*. Green **1**(2011), 5-6, 329–338.

[52] Patil A.K., Saini J.S., Kumar K.: *Heat transfer and friction characteristics of solar air heater duct roughened by broken V-shape ribs combined with staggered rib piece*. J. Renew. Sustain. Energy **4**(2012), 1, 013115.

[53] Patil A.K., Saini J.S., Kumar K.: *A comprehensive review on roughness geometries and investigation techniques used in artificially roughened solar air heaters*. Int. J. Renew. Energy Res. **2**(2012), 1, 1–15.

[54] Deo N.S., Chander S., Saini J.S.: *Performance analysis of solar air heater duct roughened with multigap V-down ribs combined with staggered ribs*. Renew. Energy **91**(2016), 484–500.

[55] Saini R.P., Saini J.S.: *Heat transfer and friction factor correlations for artificially roughened ducts with expanded metal mesh as roughness element*. Int. J. Heat Mass Transf. **40**(1997), 4, 973–986.

[56] Karmare S.V., Tikekar A.N.: *Heat transfer and friction factor correlation for artificially roughened duct with metal grit ribs*. Int. J. Heat Mass Transf. **50**(2007), 21-22: 4342–4351.

[57] Thakur S., Thakur N.S.: *Impact of multi-staggered rib parameters of the 'W'shaped roughness on the performance of a solar air heater channel*. Energ. Source Part A (2020), 1–20.

[58] Kumar K., Prajapati D.R., Sushant S.: *Heat transfer and friction factor correlations development for solar air heater duct artificially roughened with 'S' shape ribs*. Exp. Therm. Fluid Sci. **82**(2017), 249–261.

[59] Gill R.S., Hans V.S., Singh S.: *Investigations on thermo-hydraulic performance of broken arc rib in a rectangular duct of solar air heater*. Int. Commun. Heat Mass Transf. **88**(2017), 20–27.

[60] Jain S.K., Agrawal G.D., Misra R.: *Heat transfer augmentation using multiple gaps in arc-shaped ribs roughened solar air heater: An experimental study*. Energ. Source Part A **43**(2021), 24, 3345–3356.

[61] Jain S.K., Agrawal G.D., Misra R.: *Experimental investigation of thermohydraulic performance of the solar air heater having arc-shaped ribs with multiple gaps*. J. Therm. Sci. Eng. Appl. **12**(2020), 1, 011014.

[62] Jain S.K., Misra R., Agrawal G.D.: *Effect of gap width on thermal performance of solar air heater having arc-shaped ribs with symmetrical gaps: An experimental investigation*. Environ. Dev. Sustain. **22**(2020), 7, 6563–6583.